Electronic Supplementary Material (ESI) for Materials Horizons.

Supporting Information

Targeted high-precision up-converting thermometer platform over multiple temperature zones with Er^{3+}

Zhihui Rao, Zhilin Li, Xiujian Zhao, and Xiao Gong*

State Key Laboratory of Silicate Materials for Architectures, Wuhan University of Technology, Wuhan 430070, P. R. China.

* Corresponding author

E-mail: xgong@whut.edu.cn (X. Gong)

Experimental Section

Materials and chemicals: Cesium chloride (CsCl, 99.99%), Erbium oxide (Er_2O_3, 99.99%), Ytterbium oxide (Yb_2O_3, 99.9%), Sodium chloride (NaCl, 99.99%), Indium chloride ($InCl_3$, 99.99%) were purchased from Aladdin Industrial Corporation. Ethyl alcohol and hydrochloric acid (HCl, 37%) were purchased from Sinopharm Chemical Reagent Company. All chemicals were used as received without further purification.

Synthesis of $Cs_2NaInCl_6$:Er-Yb microcrystals: Samples of $Cs_2NaInCl_6$ double-perovskite microcrystals with different concentration of lanthanide were prepared by a typical synthetic. Stoichiometric amounts of related cationic halogenated salts were dissolved in a vial with 2 mL HCl via strongly stirred at 80 °C. Then CsCl powder was added as a precipitate initiator to formed a white precipitate. After the reaction was completed, the samples were thoroughly washed with ethanol and stored under suitable conditions for further study.

Measurement and Characterization: X-ray diffraction **(**XRD) patterns were recorded by an X-ray diffractometer (Empyrean) using Cu Ka radiation. Zeiss Ultra Plus was used to obtain The field emission scanning electron microscopy (FESEM) images and energy-dispersive X-ray spectroscopy mapping. X-ray photoelectron spectra (XPS) were measured with ESCALAB 250Xi photoelectron spectrometer (Thermo Electron Co., USA). To accurately determine concentration of dopants, the inductively coupled plasma optical emission spectrometry (ICP-MS) was recorded by using atomic absorption spectrometer (CONTRAA-700, Analytik Jena Co., GER).

Thermogravimetric analysis (TGA) data was performed with a simultaneous thermal analyzer (TGA/DSC2 1600LF, METTLER TOLEDO). Optical spectroscopy and temperature-dependent measurements of samples was characterized by Edinburgh Instruments FLS 1000 spectrometer, an external semiconductor NIR laser (WPL1-Y 1002-A22-98010-10.0W-R-LCD). Upconversion photoluminescence spectrum were measured by a homemade system consisting of two monochromators, photomultiplier tube, lock-in amplifier, and different wavelength light sources.

Table S1. Element content measured by ICP-MS. The molar concentration of Er^{3+} = 100%[Er]/[In], and the molar concentration of Yb^{3+} = 100%[Yb]/[In].

Samples	Precursor		Product (ICP-MS)	
	Er^{3+}	Yb^{3+}	Er^{3+}	Yb^{3+}
$Cs_2NaInCl_6$: Er-Yb	5%	20%	1.19%	2.14%
$Cs_2NaInCl_6$: Er-Yb	10%	20%	2.67%	2.19%
$Cs_2NaInCl_6$: Er-Yb	15%	20%	3.76%	2.16%
$Cs_2NaInCl_6$: Er-Yb	20%	20%	8.57%	2.66%
$Cs_2NaInCl_6$: Er-Yb	30%	20%	11.95%	2.68%
$Cs_2NaInCl_6$: Er-Yb	40%	20%	14.99%	2.43%

Table S2. EDS data of each element in Er-Yb doped samples. EDS is not accurate for the determination of trace elements, which can be combined with Table S1 to see the detailed element analysis.

Samples	Cs: Ag: In: Cl: Er: Yb Product
$Cs_2NaInCl_6$	2.13:1.09:0.97:5.80:0:0
$Cs_2NaInCl_6$:0.2Yb	2.18:1.05:0.99:5.77:0.019
$Cs_2NaInCl_6$:0.2Er	1.96:1.24:0.99:5.80:0.012
$Cs_2NaInCl_6$:0.2Er-0.2Yb	2.14:1.19:0.93:5.74:0.003:0.0

Table S3. The crystallographic data for $Cs_2NaInCl_6$.

Formula	$Cs_2NaInCl_6$
Formula weight	316.33
Crystal system	Cubic
space group	$Fm\bar{3}m$ (225)
a (=b=c) (Å)	10.5090
α(=β=γ) (degree)	90
Cell volume ($Å^3$)	1160.60
	Ref. 1

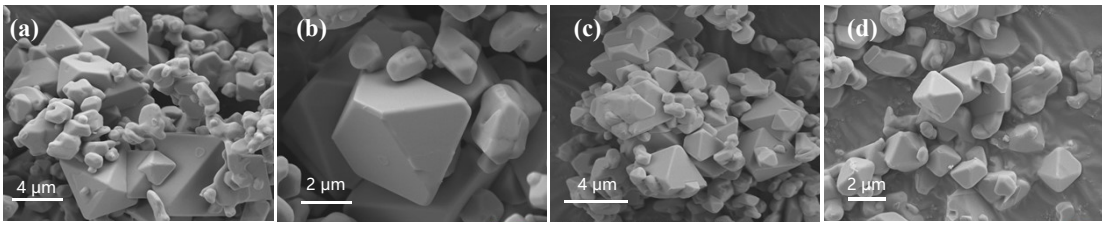

Figure S1. SEM images of $Cs_2NaInCl_6$ (a), $Cs_2NaInCl_6$:Yb (b), $Cs_2NaInCl_6$:Er (c) and $Cs_2NaInCl_6$:Er-Yb (d) microcrystal which reveals a micron-sized crystal with octahedron morphology.

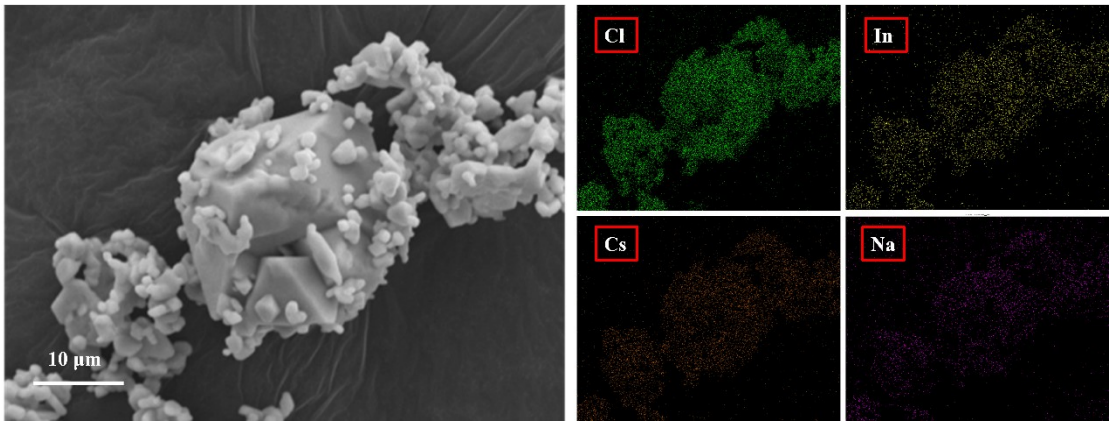

Figure S2. SEM image of $Cs_2NaInCl_6$ microcrystal and EDS mapping images showing the distribution of various elements.

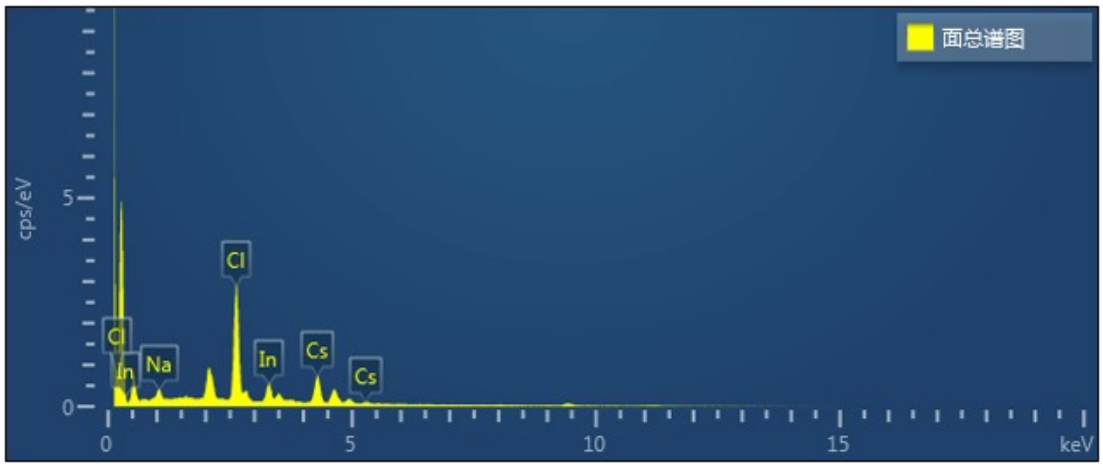

Figure S3. The EDS spectrum of $Cs_2NaInCl_6$ microcrystal.

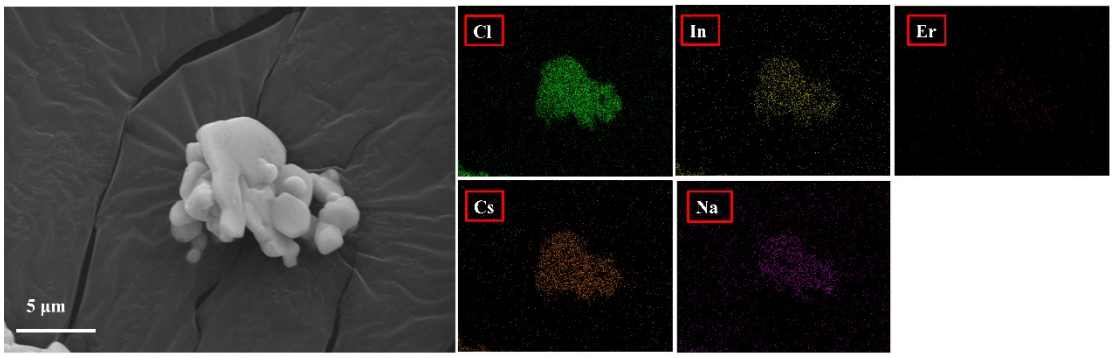

Figure S4. SEM image of $Cs_2NaInCl_6$:Er microcrystal and EDS mapping images showing the distribution of various elements.

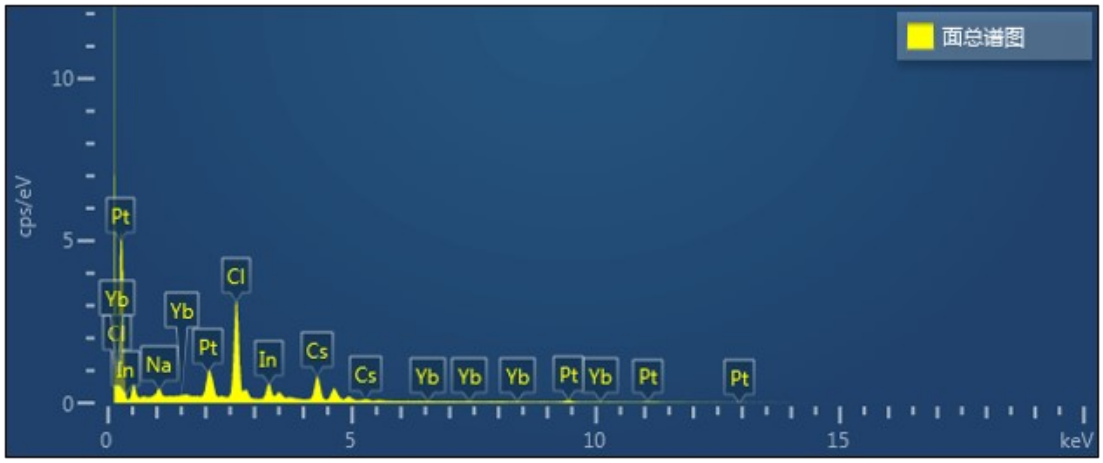

Figure S5. The EDS spectrum of $Cs_2NaInCl_6$:Er microcrystal.

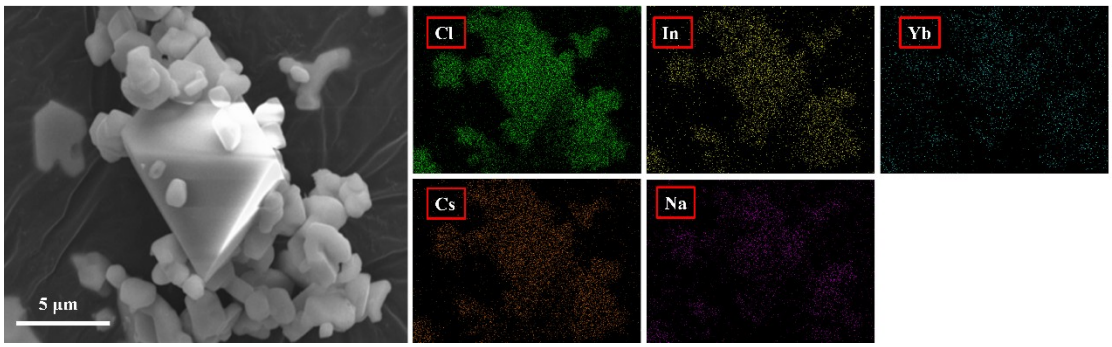

Figure S6. SEM image of $Cs_2NaInCl_6$:Yb microcrystal and EDS mapping images showing the distribution of various elements.

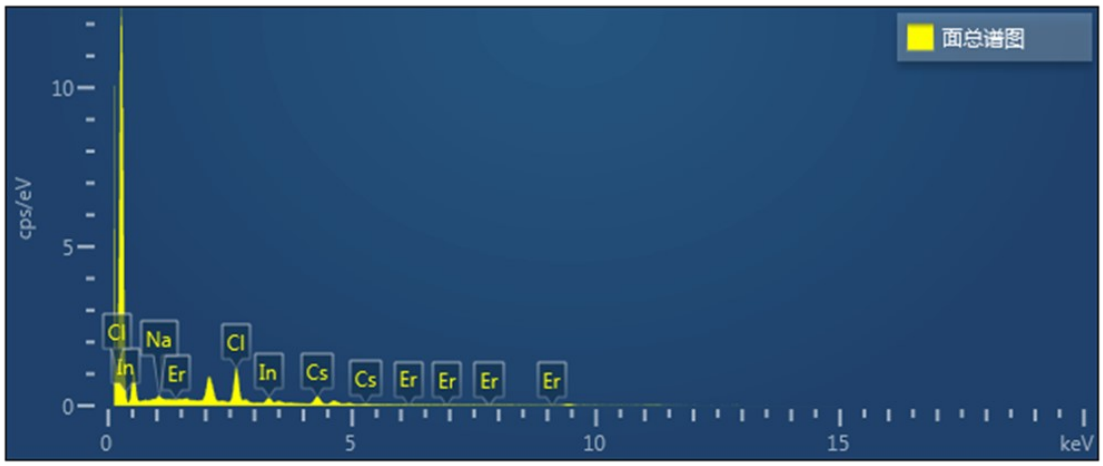

Figure S7. The EDS spectrum of $Cs_2NaInCl_6$:Yb microcrystal.

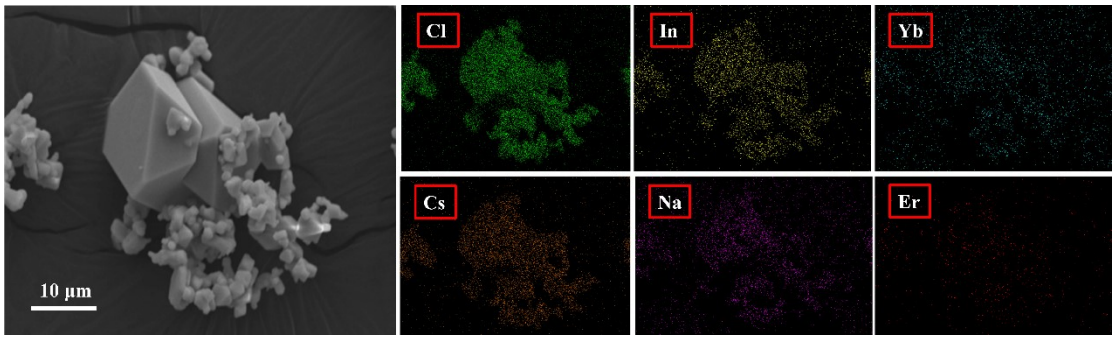

Figure S8. EM image of $Cs_2NaInCl_6$:Er-Yb microcrystal and EDS mapping images showing the distribution of various elements.

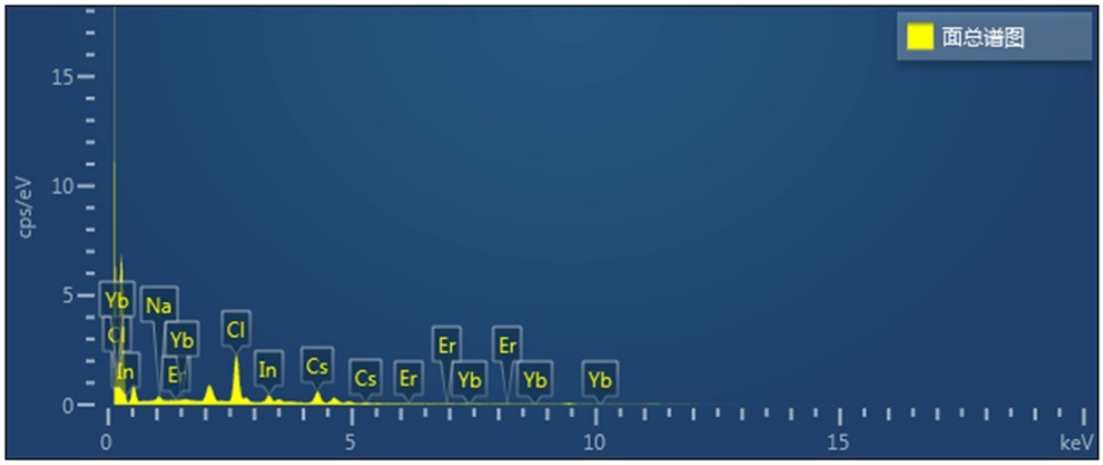

Figure S9. The EDS spectrum of $Cs_2NaInCl_6$:Er-Yb microcrystal.

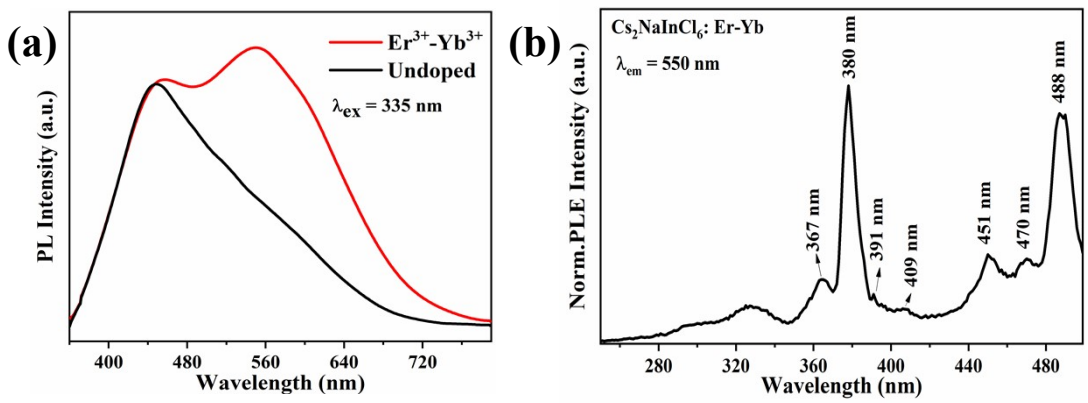

Figure S10. (a) Compared PL spectra of the undoped sample with the Er^{3+}/Yb^{3+} doped in visible region under 335 nm lamp excitation. (b) The photoluminescence excitation (PLE) of 550 nm peak.

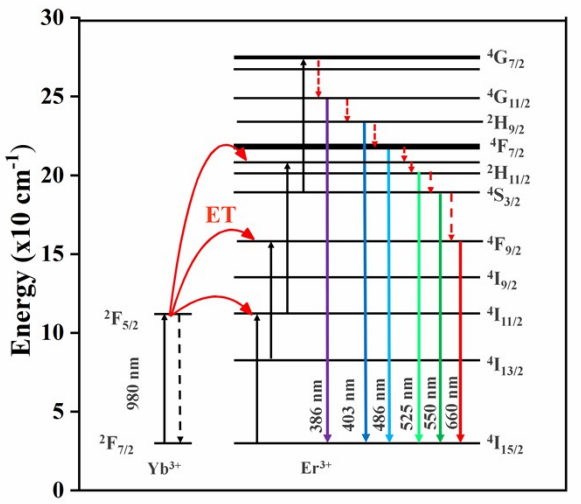

Figure S11. The simplified energy diagram and possible populating pathways of $Cs_2NaInCl_6$:Er-Yb.

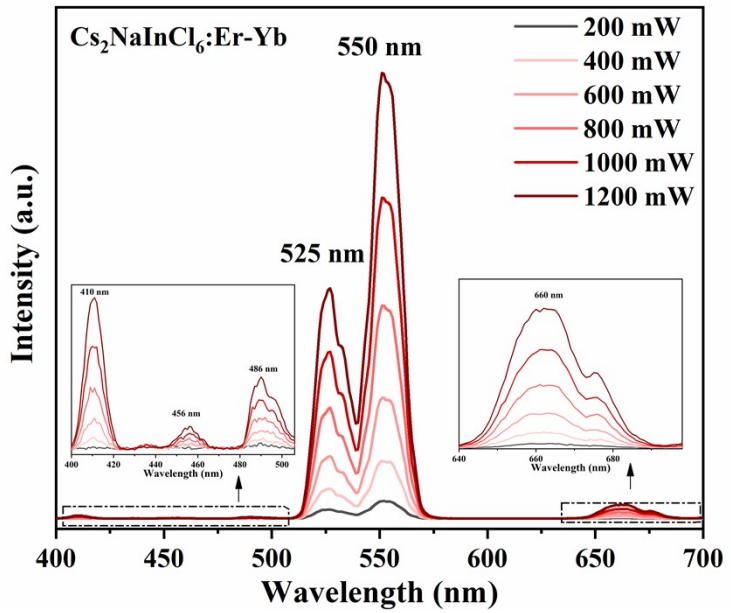

Figure S12. Pump-power dependence of upconversion luminescence intensity of $Cs_2NaInCl_6$:0.3Er-0.3Yb.

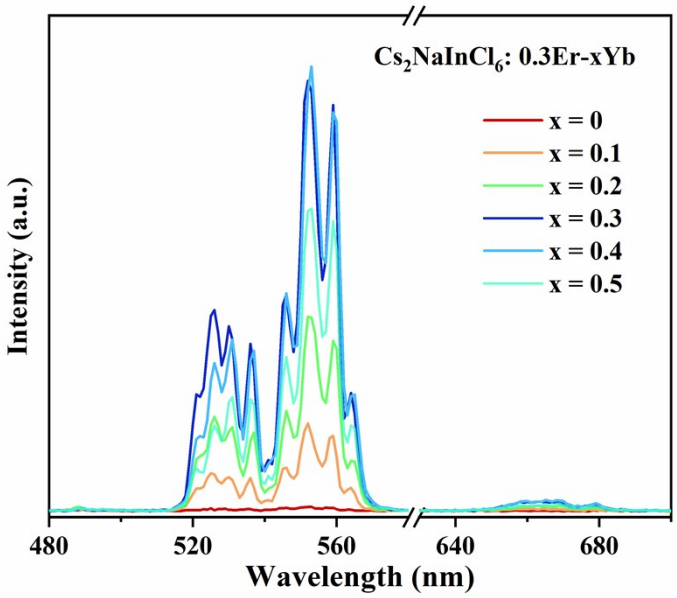

Figure S13. The upconversion PL spectra of $Cs_2NaInCl_6$:0.3Er-xYb (x = 0, 0.1, 0.2, 0.3, 0.4, 0.5).

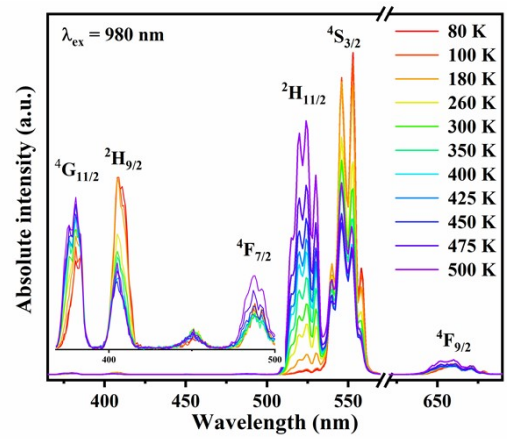

Figure S14. Full spectrum display of upconversion PL intensity versus temperature in $Cs_2NaInCl_6$:0.3Er-0.3Yb DPs.

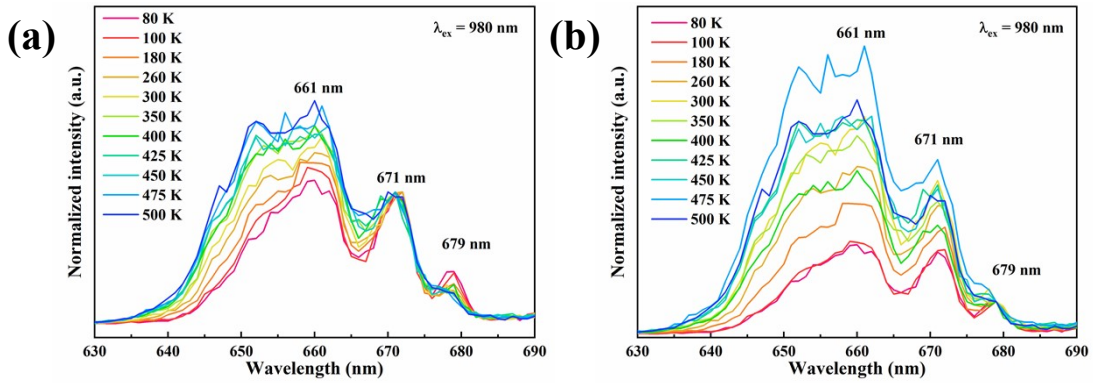

Figure S15. Boltzmann plot of the temperature-dependent FIR of Stark energy levels from $^4F_{9/2}$ crystal filed with high-resolution normalized at 671 nm (a) and 679 nm (b), repectively. Above 300 K, TCLs between 661 nm and 671 nm level or between 661 nm and 679 nm level dose not follow the Boltzmann statistics. However, when plot was normalized at 671 nm, we can find a better thermal trend in 80 K and 100 K, which is different from the trend in the diagram normalized at 679 nm. These result from smaller energy levels of between 661 nm and 671 nm level, which as candidate for temperature measurement at lower temperatures. It also proved the feasibility of our strategy to adapt to different temperature measurement intervals through the reasonable selection of energy levels.